Mitigating Bias in Calibration Error Estimation

Rebecca Roelofs
Google Research

Nicholas Cain
Google Research

Jonathon Shlens
Google Research

Michael C. Mozer
Google Research

Abstract

For an AI system to be reliable, the confidence it expresses in its decisions must match its accuracy. To assess the degree of match, examples are typically binned by confidence and the per-bin mean confidence and accuracy are compared. Most research in calibration focuses on techniques to reduce this empirical measure of calibration error, ECE_{BIN}. We instead focus on assessing statistical bias in this empirical measure, and we identify better estimators. We propose a framework through which we can compute the bias of a particular estimator for an evaluation data set of a given size. The framework involves synthesizing model outputs that have the same statistics as common neural architectures on popular data sets. We find that binning-based estimators with bins of equal mass (number of instances) have lower bias than estimators with bins of equal width. Our results indicate two reliable calibration-error estimators: the debiased estimator (Brocker, 2012; Ferro and Fricker, 2012) and a method we propose, ECE_{SWEEP}, which uses equal-mass bins and chooses the number of bins to be as large as possible while preserving monotonicity in the calibration function. With these estimators, we observe improvements in the effectiveness of recalibration methods and in the detection of model miscalibration.

1 INTRODUCTION

Machine learning models are increasingly deployed in high-stakes settings like self-driving cars (Caesar et al., 2020; Geiger et al., 2013; Sun et al., 2020) and medical diagnosis (Esteva et al., 2017, 2019; Gulshan et al., 2016) where it is critical to recognize when a model is likely to be incorrect. Unfortunately, models often fail in unexpected and poorly understood ways, hindering our ability to interpret and trust such systems (Azulay and Weiss, 2018; Biggio and Roli, 2018; Hendrycks and Dietterich, 2019; Recht et al., 2019; Szegedy et al., 2013). To address these issues, calibration is used to ensure that a model produces confidence scores that reflect its ground truth likelihood of being correct (Platt et al., 1999; Zadrozny and Elkan, 2001, 2002).

To obtain an estimate of the calibration error, or ECE[1], the standard procedure partitions the model confidence scores into bins and compares the model's predicted accuracy to its empirical accuracy within each bin (Guo et al., 2017; Naeini et al., 2015). We refer to this specific metric as ECE_{BIN}. Recent work observed that the calculation of ECE_{BIN} is sensitive to implementation (Kumar et al., 2019; Nixon et al., 2019). Fundamentally, a key confounding factor is *statistical bias*, the difference between the expected ECE_{BIN} and the true calibration error (TCE). Because bias is largely unexplored in the literature, its magnitude and sign is unknown, as is its dependence on hyperparameters of the ECE_{BIN} estimator (e.g., number of bins, how bins are formed). We explain our reasons for focusing on estimator bias and not variance in Section 4.

Bias in ECE_{BIN} measurement has two real world consequences. First, the measurement of calibration error on a given model may be systematically incorrect. Thus, our understanding of how well a model knows whether it is correct may be poor, and may not be accurately captured by naively reporting ECE_{BIN}. Second, many techniques have been developed to minimize the calibration error, such as post-hoc recalibration techniques (Guo et al., 2017; Zadrozny and Elkan, 2001, 2002) and, more recently, calibration-sensitive training objectives (Karandikar et al., 2021; Krishnan and Tickoo, 2020; Kumar et al., 2018; Lin et al., 2018; Mukhoti et al., 2020). Given that the selection of the training objectives and the justification of a recalibration technique is predicated on the measurement of the calibration

---

[1] Naeini et al. (2015) introduce ECE as an acronym for *Expected* Calibration Error. However, ECE is not a proper expectation whereas the true calibration error is computed under an expectation. To resolve this confusion, we prefer to read ECE as *Estimated* Calibration Error.
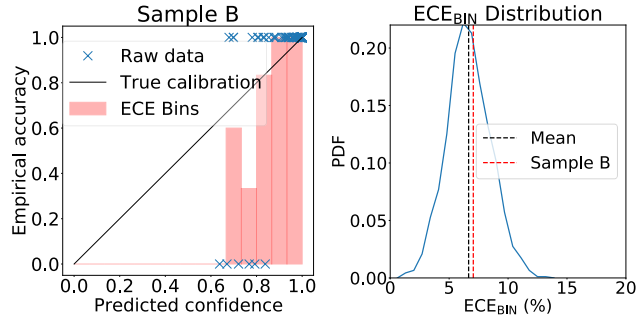
(a) Figure 1: ECE_{BIN} exhibits large bias for perfectly calibrated models. We simulate data from a perfectly calibrated model with confidence scores fit to ResNet-110 CIFAR-10 output (He et al., 2016; Kängsepp, 2019) and measure ECE_{BIN} using 15 equal-width-spaced bins. The left panel shows a reliability diagram for a sample of size $n = 200$ (named Sample B); the right panel has a distribution of ECE_{BIN} scores computed across 10^6 independent simulations. *Even though the model is perfectly calibrated, ECE_{BIN} systematically predicts large calibration errors.*

error, reliance on an inaccurate estimator may lead to a suboptimal choice.

We address this problem by developing a technique to measure bias in calibration metrics, which we call the *bias-by-construction (BBC)* framework. The BBC framework uses simulation to create a setting where the TCE can be computed analytically and thus the bias can be estimated directly. BBC reveals that ECE_{BIN} has systematic non-negligible statistical bias, particularly for perfectly calibrated models (Figure 1).

Our goal is to identify the least biased estimator of calibration error using BBC. We consider two estimators previously proposed in the literature: the *debiased* estimator (Brocker, 2012; Ferro and Fricker, 2012), which we refer to as ECE_{DEBIAS}, and the smoothed kernel density estimator of Zhang et al. (2020), which we refer to as *KDE*. Additionally, we propose an extension of ECE_{BIN} where the number of bins is chosen to ensure monotonicity of the calibration histogram, which we refer to as ECE_{SWEEP}. ECE_{BIN}, $\text{ECE}_{\text{DEBIAS}}$, and $\text{ECE}_{\text{SWEEP}}$ all require the binning of model confidence scores, and under the lens of bias, we examine two common methods for specifying bins: partitioning the confidence-score continuum either into *equal width* bins or bins of *equal mass*—equal numbers of data instances.

Furthermore, BBC allows us to examine the impact of biased estimators in downstream decision making, such as the selection of a post-hoc recalibration method. For example, when the choices for recalibration include histogram binning (Zadrozny and Elkan, 2001), temperature scaling (Guo et al., 2017), and isotonic regression (Zadrozny and Elkan, 2002), Table 1 illustrates that

our bias-reduced measure, $\text{ECE}_{\text{SWEEP}}$, more frequently selects the 'optimal' recalibration method when compared to the standard measure, ECE_{BIN} (70% versus 30% correctness, respectively). Optimality is determined by estimating TCE using numerical integration on curves arising from maximum likelihood fits across multiple model families, where we select the best model via the Akaike information criterion (see Section 6).

To summarize the contributions of this work, the core contribution is a simulation framework, bias by construction or BBC, that allows us to identify and characterize systematic bias in calibration error metrics for realistic models and data sets. We show that estimation of calibration error by the predominant method, ECE_{BIN}, is biased, and paradoxically the bias is most severe for perfectly calibrated models. Bias can lead not only to the mis-estimation of calibration error but also to the wrong choice of recalibration method, yielding a poorly calibrated model. Moreover, we find that the selection of hyperparameters for measuring calibration (e.g., number of bins) is under-appreciated and is absolutely critical. To address these issues, we propose $\text{ECE}_{\text{SWEEP}}$, a simple algorithm based on the monotonicity principle of calibration curves. We compare the bias of various estimators using predictions from four popular neural architectures and three data sets. We find that ECE_{BIN} is more biased than either $\text{ECE}_{\text{DEBIAS}}$ or $\text{ECE}_{\text{SWEEP}}$, and of these two improved measures, $\text{ECE}_{\text{DEBIAS}}$ performs better for perfectly calibrated models and $\text{ECE}_{\text{SWEEP}}$ for miscalibrated models. Finally, our analyses provide rigorous empirical evidence that for all binning-based estimators, equal-mass binning obtains a more accurate estimate of true calibration error. This finding gives strong guidance to revise the current practice of equal-width binning.

2 RELATED WORK

ECE_{BIN}. ECE_{BIN} with 15 bins of equal width is currently the most popular way to measure calibration error in the literature (Guo et al., 2017; Naeini et al., 2015). An alternative but less popular implementation evaluates ECE_{BIN} using bins of equal mass, which partitions examples into bins that have an equal number of examples (Kumar et al. (2019); Zadrozny and Elkan (2001). Recently, Nixon et al. (2019) observed that ECE_{BIN} with equal-mass-binning produces more stable rankings of recalibration algorithms, which is consistent with our conclusion that equal mass ECE_{BIN} is a less biased estimator of TCE.

Sensitivity of ECE_{BIN} to implementation hyperparameters. Several works have pointed out that ECE_{BIN} is sensitive to implementation details. Kumar et al. (2019) show that ECE_{BIN} increases with number of bins. Nixon et al. (2019) find that ECE_{BIN} is sen-

	CIFAR-10				CIFAR-100				ImageNet	
	ResNet 110	ResNet 110_SD	WideResNet 32	DenseNet 40	ResNet 110	ResNet 110_SD	DenseNet 40	WideResNet 32	ResNet 152	DenseNet 161
ECE_{BIN}	✗	✓	✗	✓	✗	✓	✗	✗	✗	✗
$\text{ECE}_{\text{SWEEP}}$	✓	✓	✓	✓	✗	✓	✓	✓	✗	✗

Table 1: The selection of a recalibration method is severely affected by biased computational methods. For ten models, we report whether either ECE_{BIN} or $\text{ECE}_{\text{SWEEP}}$ select the same (✓) or different (✗) recalibration algorithm (either histogram binning, isotonic regression or temperature scaling) as would an estimate of TCE obtained from maximum likelihood fits to empirical data (see Section 6). ECE_{BIN} selects the same algorithm only 3/10 times, versus 7/10 for $\text{ECE}_{\text{SWEEP}}$, illustrating how computational bias can negatively impact recalibration.

sitive to several hyperparameters, including ℓ_p norm, number of bins, and binning technique. In contrast to prior work, we explicitly quantify estimation bias in simulation for realistic model outputs, and we show precisely how the *bias* in ECE_{BIN} varies with the choice of sample size, model architecture, datasets, and implementation hyperparameters for ECE_{BIN} such as number of bins and binning method.

Less biased metrics for calibration error. Motivated by the sensitivity of ECE_{BIN} to implementation hyperparameters, recent work has proposed less biased estimates of TCE. In particular, Ferro and Fricker (2012) and Brocker (2012) propose a *debiased estimator*, $\text{ECE}_{\text{DEBIAS}}$, which uses a jackknife technique to estimate the per-bin bias in the standard ECE_{BIN}, and subtracts off this bias to achieve a better binned estimate of the calibration error. Similarly, Zhang et al. (2020) propose a smoothed Kernel Density Estimation (KDE) method for reducing bias when estimating calibration error. Relative to $\text{ECE}_{\text{SWEEP}}$, both $\text{ECE}_{\text{DEBIAS}}$ and KDE have an additional hyperparameter (number of bins or kernel bandwidth, respectively). We compare $\text{ECE}_{\text{SWEEP}}$, $\text{ECE}_{\text{DEBIAS}}$, and KDE, finding circumstances in which $\text{ECE}_{\text{SWEEP}}$ and $\text{ECE}_{\text{DEBIAS}}$ have relative advantages in bias reduction.

Alternative definitions of calibration error. Researchers have studied alternatives notions of calibration error that are distinct from TCE (see Section 3 for a formal definition of TCE). For example, Widmann et al. (2019) proposed a kernel-based calibration error, KCE, which has no explicit dependence on the model's calibration function. Gupta et al. (2020) propose a calibration error metric inspired by the Kolmogorov-Smirnov (KS) statistical test that estimates the maximum difference between cumulative probability distributions describing the model's confidence and accuracy. The KS is similar to the maximum calibration error (MCE) (Naeini et al., 2015) in that it computes a worst-case deviation between confidence and accuracy, but the KS is computed on the CDF, while the MCE uses binning and is computed on the PDF. In contrast, TCE measures the *average* difference between confi-

dence and accuracy. Both the worst case and average difference are useful measures but may be applicable under different circumstances (Guo et al., 2017).

Monotonicity in calibration curves. While Zadrozny and Elkan (2002) used calibration curve monotonicity to motivate isotonic regression for recalibration, they observed monotonic calibration curves empirically on only a handful of pre-deep learning models, and without theoretical justification. In contrast, our work is the first to suggest using monotonicity to improve *calibration metrics*. We provide both theoretical and extensive empirical evidence that monotonic calibration curves arise in modern deep networks.

3 BACKGROUND

Consider a binary classification setup with input $X \in \mathcal{X}$, target output $Y = \{0, 1\}$, and suppose we have a model $f : X \to [0, 1]$ whose output represents a confidence score that the true label Y is 1.

True calibration error (TCE). We define true calibration error as the ℓ_p norm difference between a model's predicted confidence and the true likelihood of being correct:[2]

$$\text{TCE}(f) = \left(\mathbb{E}_X \left[|f(X) - \mathbb{E}_Y[Y|f(X)]|^p \right] \right)^{\frac{1}{p}}. \quad (1)$$

Two independent features of a model determine TCE: (1) the distribution of confidence scores $f(x) \sim \mathcal{F}$ over which the outer expectation is computed, and (2) the true calibration curve $\mathbb{E}_Y[Y \mid f(X)]$, which governs the relationship between the confidence score $f(x)$ and the empirical accuracy (see Figure 2a for illustration).

3.1 Estimates of calibration error

To estimate the TCE of a model f, assume we are given a dataset containing n samples, $\{x_i, y_i\}_{i=1}^n$. We can approximate TCE by replacing the outer expectation in Equation 1 by the sample average and replacing the

---

[2]In our experiments, we measure calibration error using the ℓ_2 norm because it increases the sensitivity of the error metric to extremely poorly calibrated predictions, which tend to be more harmful in applications.
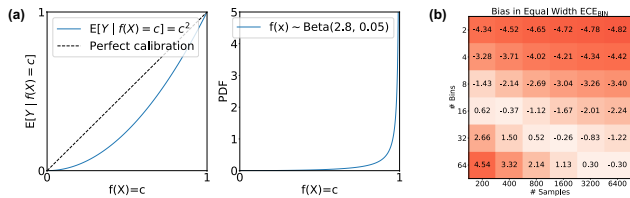
Figure 2: (a) Curves controlling true calibration error. Our ability to measure calibration is contingent on both the confidence score distribution (e.g., $f(X) \sim$ Beta$(2.8, 0.05)$) and the true calibration curve (e.g., $\mathbb{E}_Y[Y \mid f(X) = c] = c^2$. (b) ECE$_{\text{BIN}}$ may underestimate or overestimate TCE. The number of bins with minimal bias grows with the sample size.

inner expectation with an average over instances with similar $f(x)$ values:

$$\text{ECE}_{\mathcal{N}}(f) = \left(\frac{1}{n} \sum_{i=1}^{n} \left| f(x_i) - \frac{1}{|\mathcal{N}_i|} \sum_{j \in \mathcal{N}_i} y_j \right|^p \right)^{\frac{1}{p}},$$ (2)

where $\mathcal{N}_i$ is instance i's set of neighbors in model confidence output space.

Label-binned calibration error (ECE$_{\text{LB}}$). Label-binned calibration error uses binning to define $\mathcal{N}_i$ and estimate the model's empirical accuracy $\mathbb{E}[Y|f(X)]$. The instances are partitioned into b bins, where B_k denotes the set of all instances in bin k, expressing Equation 2 in terms of the binned neighborhood:

$$\text{ECE}_{\text{LB}}(f) = \left(\frac{1}{n} \sum_{k=1}^{b} \sum_{i \in B_k} |f(x_i) - \bar{y}_k|^p \right)^{\frac{1}{p}},$$
$$\text{where } \bar{y}_k = \frac{1}{|B_k|} \sum_{j \in B_k} y_j.$$ (3)

Binned calibration error (ECE$_{\text{BIN}}$). In contrast to ECE$_{\text{LB}}$, which operates on the original instances but uses binning to estimate empirical accuracy, ECE$_{\text{BIN}}$ collapses all instances in a bin together and compares the per-bin empirical accuracy to the per-bin confidence score, weighted by the per-bin instance count. Given b bins, where B_k is the set of instances in bin k, and letting $\bar{f}_k$ and $\bar{y}_k$ be the per-bin average confidence score and label, ECE$_{\text{BIN}}$ is defined under the ℓ_p norm:

$$\text{ECE}_{\text{BIN}}(f) = \left(\sum_{k=1}^{b} \frac{|B_k|}{n} \left| \bar{f}_k - \bar{y}_k \right|^p \right)^{\frac{1}{p}}$$ (4)

Importantly, $\text{ECE}_{\text{LB}}(f) \geq \text{ECE}_{\text{BIN}}(f)$, which follows by applying Jensen's inequality on each inner term $k \in \{1, 2, \ldots, b\}$ in Eqs. 3 and 4:

$$\frac{1}{|B_k|} \sum_{i \in B_k} |f(X_i) - \bar{Y}_k|^p \geq \left| \sum_{i \in B_k} \bar{f}_k - \bar{Y}_k \right|^p.$$ (5)

4 THE BBC FRAMEWORK

We focus on bias rather than variance because the variance can be estimated from a finite set of samples

through resampling techniques whereas the bias is an unknown quantity that reflects systematic error. For completeness, we report variance for various calibration metrics as we vary the sample size, number of bins, and binning technique in Appendix B. We find empirically that the variance is relatively insensitive to the estimation technique and number of bins.

The *bias* of a calibration error estimator, ECE$_{\mathcal{A}}$ for some estimation algorithm $\mathcal{A}$, is the difference between the estimator's expected value with respect to the data distribution and the TCE:

$$\text{Bias}_{\mathcal{A}} = \mathbb{E}[\text{ECE}_{\mathcal{A}}] - \text{TCE}.$$ (6)

If we assume a specific confidence score distribution $\mathcal{F}$ and true calibration curve $T(X) = \mathbb{E}_Y[Y \mid f(X) = c]$ (see Figure 2a for examples), we can compute the TCE by analytically or numerically evaluating the integral implicit in the outer expected value of Equation 1. We then compute a sample estimate of the bias by generating n samples $\{f(x_i), y_i\}_{i=1}^{n}$ such that $f(x_i) \sim \mathcal{F}$ and $\mathbb{E}_Y[Y \mid f(X) = c] := T(c)$, and computing the ECE on the sample. We repeat this process for m simulated datasets and compute the sample estimate of bias (hereafter, simply the "bias") as the difference between the average ECE and the TCE:

$$\widehat{\text{Bias}}_{\mathcal{A}}(n) = \frac{1}{m} \sum_{i=1}^{m} \text{ECE}_{\mathcal{A}} - \text{TCE}.$$ (7)

Using this *bias-by-construction (BBC)* framework, we next investigate the bias in ECE$_{\text{BIN}}$ as a function of the number of samples n and the number of bins. We compute ECE$_{\text{BIN}}$ with equal width binning and we assume parametric curves for $f(x)$ and $\mathbb{E}_Y[Y \mid f(X)]$ that are fit to the ResNet-110 CIFAR-10 model output. (Section 6 has details on how we compute fits.)

Proposition 3.3 of Kumar et al. (2019) asserts that any binned version of calibration error systematically underestimates TCE *in the limit of infinite data*. However, for a finite number of samples n, Figure 2b shows that ECE$_{\text{BIN}}$ can either overestimate or underestimate TCE and that increasing the number of bins does not always lead to better estimates of TCE. In Appendix B, we show how bias and variance vary for several calibration metrics as we change the binning scheme, sample size, and number of bins. Regardless of binning scheme, for ECE$_{\text{BIN}}$ we find empirically that *there exists a bin number for each sample size that results in the lowest estimation bias and this optimal bin count grows with the sample size.* Intuitively, having a large number of bins is generally preferred because we can obtain a finer-resolution estimate of the calibration curve. However, if we have a small number of samples, setting the number of bins too high may result in a poor estimate of the calibration curve due to the low number of samples in each bin.

5 MONOTONIC CALIBRATION METRICS

Though Section 4 shows that there exists an optimal number of bins for which ECE_{BIN} has the lowest bias, unfortunately, this number depends on the binning technique, the number of samples, the confidence score distribution, and the true calibration curve. This observation motivates us to seek a method for adaptively choosing the number of bins.

Monotonicity in the true calibration curve implies that a model's expected accuracy should not decrease as the model's confidence increases. Although this requirement seems reasonable for any statistical model, it is not obvious how to prove why or when a "reasonable" model would attain such a property. We offer a rationale for why it should be expected of machine learning models trained with a maximum likelihood objective, e.g., cross-entropy or logistic loss. Namely, from ROC (receiver operating characteristic) analysis of maximum likelihood models, an under-appreciated observation of ROC curves is that a model trained to maximize the likelihood ratio must have a convex ROC curve in the limit of infinite data (see Green et al., 1966, Sec. 2.3). The slope of the ROC curve is related to the calibration curve, and a convex ROC curve implies a monotonically increasing calibration curve (the converse is also true) (Chen et al., 2018; Gneiting and Vogel, 2018).

In practice, several potential confounds may lead to observing non-monontonic calibration curves. First, finite data size may lead to fluctuations in the true positive or false positive rates, but do not reflect the behavior of the underlying model. Second, deviations in domain statistics between cross-validated splits in the data may lead to unbounded behavior; however, we assume that such domain shifts are negligible as cross-validated splits are presumed to be selected *i.i.d.*[3] Given that deviations from non-monotonic calibration curves are considered artificial, we posit that any method that is trying to assess the TCE of an underlying model may freely assume monotonicity in the true calibration curve. Note that this proposition already guides the entire field of re-calibration to require that re-calibration methods only consider monotonic functions (Platt et al., 1999; Wu et al., 2012; Zadrozny and Elkan, 2002).

Accordingly, we leverage underlying monotonicity in the true calibration curve and propose the *monotonic sweep calibration error*, a metric that chooses the largest

---

[3]Note that a third potential reason for a non-monotonic calibration curve is that a classifier could be trained with a non–likelihood-based statistical criteria, e.g. moment matching. However, a lack of monotonic behavior in the calibration curve of such a model may actually be a sign that the model is not reasonable or admissible model on a given task (Chen et al., 2018; Pesce et al., 2010).

---

number of bins possible such that the chosen bin size and all smaller bin sizes preserve monotonicity in the bin heights $\bar{y}_k$, i.e.,

$$\text{ECE}_{\text{SWEEP}} = \left(\sum_{k=1}^{b^*} \frac{|B_k|}{n} \left| \bar{f}_k - \bar{y}_k \right|^p \right)^{\frac{1}{p}} \text{ where}$$
$$b^* = \max\{b \mid 1 \leq b \leq n; \forall\, b' \leq b,\ \bar{y}_1 \leq \ldots \leq \bar{y}_{b'}\} \tag{8}$$

Algorithm 1 Monotonic Sweep Calibration Error

> **for** $b = 2$ **to** n **do**
>   Compute bin heights $(\bar{y}_k)$ for ECE_{BIN} using b bins
>   **if** binning is not monotonic **then**
> $b \leftarrow b - 1$
>   **break**
>   **end if**
> **end for**
> **return** ECE_{BIN} computed with b bins

We compute the monotonic sweep calibration error by starting with $b = 2$ bins ($b = 1$ is guaranteed to be a monotonic binning) and gradually increasing the number of bins until we either reach a non-monotonic binning, in which case we return the last b that corresponded to a monotonic binning, or until every sample belongs to its own bin ($b = n$). In Appendix D, we explore the number of bins chosen by $\text{ECE}_{\text{SWEEP}}$ for varying sample sizes and model output.

6 FITTING THE CALIBRATION CURVE AND SCORE DISTRIBUTION

TCE is analytically computable when we assume parametric forms for the confidence distribution and the true calibration curve. In order to ensure that the parametric forms we use in simulation reflect the diversity and complexity of realistic model output, we develop parametric models of empirical logit datasets.

We consider 10 publicly available logit datasets (Kängsepp, 2019) that arise from training four different architectures (ResNet, ResNet-SD, Wide-ResNet, and DenseNet) (He et al., 2016; Huang et al., 2017, 2016; LeCun et al., 1998; Zagoruyko and Komodakis, 2016) on three different image datasets (CIFAR-10/100 and ImageNet) (Deng et al., 2009; Krizhevsky and Hinton, 2009). For each example in a given dataset, we compute top-label confidence scores by selecting the maximum softmax score across all classes and we compute whether or not the example resulted in a "hit," i.e. whether the model's predicted class corresponds to the true class. By using only the top-label confidence score and determining whether the top and true labels match, we can treat the calibration problem as binary.

For the parametric fits, we model confidence score distributions $f(X)$ using a beta density fit via maximum
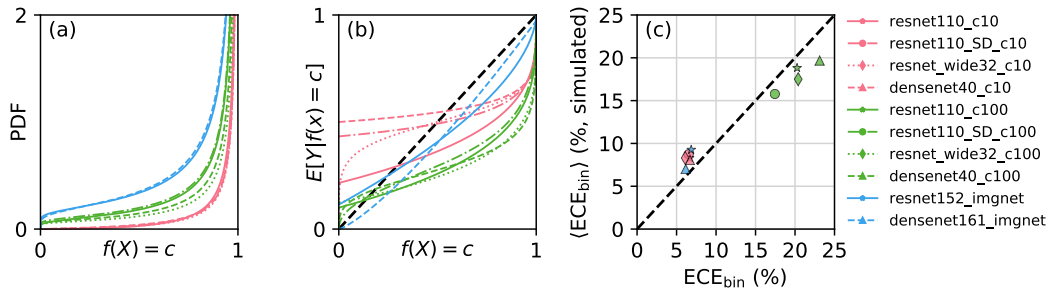
Figure 3: Maximum likelihood fits to empirical datasets illustrate large skew in their density distribution and calibration function. For each dataset, we fit (a) confidence distributions with Beta distribution and (b) calibration curves with generalized linear models across multiple model families, selecting the best model via the Akaike information criterion (details in Appendix A). We find the dataset source has a greater influence over the curves than the model architecture. (c) We plot the overall quality of the fits by computing the ECE_{BIN} on the original data vs. the ECE_{BIN} averaged over 1000 simulated trials. Curves well-fit to the data lie close to the identity line.

likelihood estimation. The beta distribution is a flexible continuous probability distributions on the interval [0,1], which makes it a natural choice for representing the probability distribution defined by the model output. For calibration curves, we fit multiple (binary) generalized linear models (GLM) to the top-label output and then select the best model using the Akaike Information Criteria (AIC). The AIC is a standard procedure for model selection in the literature, for selecting the model that most adequately describes data arising from a mechanism included in the model family. The GLM models considered include logit, log, and "logflip" ($\log(1 - x)$) link and transformation functions, up to first order in the transformed domain, which all result in monotonic calibration functions. See Appendix A for additional details.

We find that the parametric forms for the calibration curve and distribution of scores are well captured by simple GLM and beta models. Figures 3a,b show the resulting fits with parameters summarized in Appendix A. We observe significant skew in the score distribution which, as discussed in Section 7.1, poses a challenge to measuring calibration error with equal-width bins. We find that the dataset has more influence on the fits than the neural model, with ImageNet models the least skewed and CIFAR-10 the most (correlating with model accuracy). Figure 3c demonstrates that ECE_{BIN} scores computed on simulated data from the fits closely match ECE_{BIN} scores computed on the real data.

7   RESULTS

7.1   Estimating bias on real models and data

Our bias-by-construction (BBC) framework uses the parametric fits to real models and datasets from Section 6 to estimate bias as follows. Each fit permits the analytical or numerical computation of TCE and can also be used in generative fashion to draw a synthetic set of examples. ECE can then be estimated from these samples, and the difference between the estimated ECE and TCE across many samples—1,000 in results to be presented—yields the bias (Equation 7).

We estimate bias for ECE_{BIN}, $\text{ECE}_{\text{DEBIAS}}$, and $\text{ECE}_{\text{SWEEP}}$ using both equal-mass and equal-width binning, and also for the KDE estimator. Following Guo et al. (2017), we choose 15 bins for ECE_{BIN} and $\text{ECE}_{\text{DEBIAS}}$. (Appendix B includes an analysis that varies the number of bins and finds that the optimal number of bins for bias minimization depends on the number of samples. This Appendix also includes calculations of variance across estimators, bin numbers, and sample sizes.)

Figure 4 plots the bias versus sample size for seven estimators, shown separately for each of three datasets. Because the curves for individual architectures look very similar to one another for a given data set, we have averaged over model architectures. The black dotted line indicates an unbiased estimator.

Equal-width versus equal-mass binning. The dashed and solid lines correspond to equal width (EW) and equal mass (EM) bins, respectively, and the colors indicate the metric. For the three binning-based metrics, EM consistently obtains a smaller magnitude bias than EW. This finding is not well appreciated in the literature: EW is the common practice. For instance, Kumar et al. (2019) proposed $\text{ECE}_{\text{DEBIAS}}^{\text{EW}}$ and did not consider $\text{ECE}_{\text{DEBIAS}}^{\text{EM}}$. However, our results show that $\text{ECE}_{\text{DEBIAS}}^{\text{EM}}$ is a consistently less biased estimator than $\text{ECE}_{\text{DEBIAS}}^{\text{EW}}$. Our work therefore provides immediate and strong guidance to researchers and practitioners concerned with model calibration. An explanation for the advantage of EM over EW stems from the fact that, as shown in Figure 3a, models trained on CIFAR-10 and CIFAR-100 have highly skewed confidence distributions. Consequently, EW binning places most instances in the top bin. As we increase the number of samples,
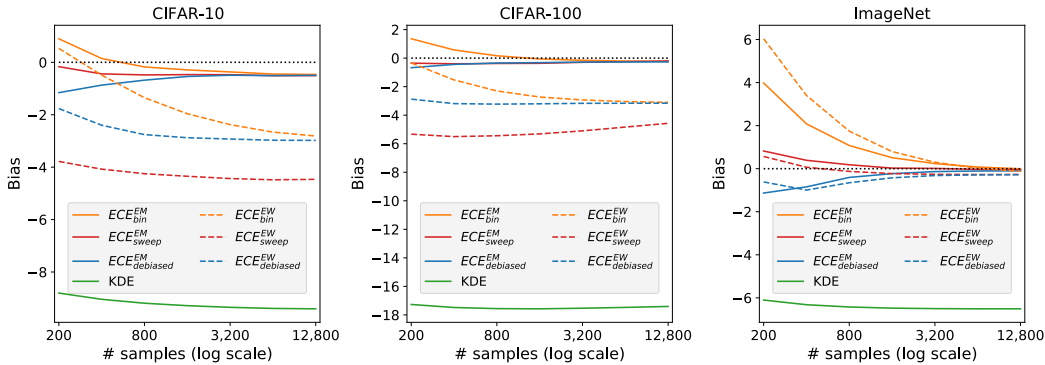
Figure 4: $\text{ECE}_{\text{SWEEP}}^{\text{EM}}$ is less biased than alternative calibration metrics. We plot bias versus number of samples n for calibration metrics on simulated data drawn from the CIFAR-10, CIFAR-100, and ImageNet fits (Section 6). The dataset the model was trained on has a greater influence on bias than the model architecture. Metrics based on equal mass binning consistently outperform equal width binning. Exploiting monotonicity in the $\text{ECE}_{\text{SWEEP}}^{\text{EM}}$ metric helps the most at small sample sizes.

we increase the likelihood that we generate a sample that populates one of the lower bins, which, due to their low sample density, may have a poorer average estimate of the TCE. On ImageNet, where the confidence distribution is less skewed, the advantage of EM over EW is still consistent but less pronounced.

Comparing metrics. Across the three datasets and various sample sizes, $\text{ECE}_{\text{SWEEP}}^{\text{EM}}$ appears to perform best. $\text{ECE}_{\text{DEBIAS}}^{\text{EM}}$ also performs well but not as well as $\text{ECE}_{\text{SWEEP}}^{\text{EM}}$ at low sample sizes. To determine whether the difference between $\text{ECE}_{\text{SWEEP}}^{\text{EM}}$ and $\text{ECE}_{\text{DEBIAS}}^{\text{EM}}$ is statistically reliable, we conducted a paired t-test on absolute bias. Across datasets, models, and number of samples, we find a statistically significant difference: a mean absolute bias is 0.504 for $\text{ECE}_{\text{DEBIAS}}^{\text{EM}}$ and 0.347 for $\text{ECE}_{\text{SWEEP}}^{\text{EM}}$ (t = 5.10, p < 1e−5). Appendix B demonstrates higher variance for $\text{ECE}_{\text{DEBIAS}}^{\text{EM}}$ than $\text{ECE}_{\text{SWEEP}}^{\text{EM}}$.

The KDE metric has much larger bias across the three datasets than any of the other metrics. This finding suggests that the heuristic used to choose the kernel bandwidth and the specific 'triweight' kernel worked well for the synthetic example evaluated in Zhang et al. (2020), but fails to generalize to the more realistic examples we study. Specifically, Zhang et al. (2020) assume a Gaussian distribution for $P(X|Y)$ and a logistic confidence score distribution, which result in notably different qualitative shapes than the logit distributions we obtain from models trained on CIFAR-10/100 or ImageNet (see Figure 3a,b or the reliability diagrams and score distributions of Kängsepp, 2019).

7.2 How well can we detect miscalibration?

Pragmatically, practitioners may be less concerned about bias per se than being able to answer a straightforward question about a model: is the model miscalibrated? If the validation set provides clear evidence of

miscalibration, further steps must be taken to correct the miscalibration. However, given bias in the ECE metrics, the mere observation of an ECE > 0 is not sufficient to raise alarm.

Consider the situation with a model of unknown TCE, and we wish to perform hypothesis testing to determine if we can reject the null hypothesis that TCE=0. Our ability to detect miscalibration depends on TCE, the sample size (n), and the method for estimating calibration error. We conduct a simulation with $f(x) \sim \text{Beta}(1, 1)$ and true calibration curve from the family $\mathbb{E}_Y[Y \mid f(X) = c] = c^d$, where d is varied to obtain a range of TCE. Allowing for a type I error rate of .05 (also known as the false-alarm rate, or the rate of mistakenly claiming miscalibration despite perfect calibration), we obtain type II error rates (also known as the miss rate, or the rate of failing to detect a miscalibration). Figure 5 shows the type II error rate as a function of TCE and n for the metric typically used in practice ($\text{ECE}_{\text{BIN}}^{\text{EW}}$) and the best performing metric identified in the previous section ($\text{ECE}_{\text{SWEEP}}^{\text{EM}}$). $\text{ECE}_{\text{SWEEP}}^{\text{EM}}$ obtains a significantly lower failure rate than $\text{ECE}_{\text{BIN}}^{\text{EW}}$, particularly for under 10,000 samples. More generally, we note limitations with both methods: to detect a miscalibration of 2%, over 10,000 samples are needed;
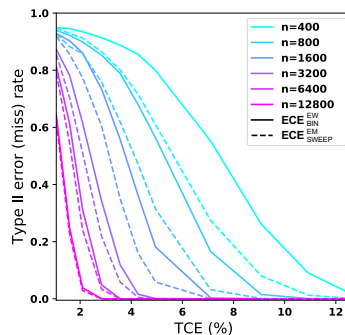

Figure 5: Probability of failing to detect miscalibration (miss rate) as a function of TCE and sample size (n). $\text{ECE}_{\text{SWEEP}}^{\text{EM}}$ has lower failure rate than $\text{ECE}_{\text{BIN}}^{\text{EW}}$.
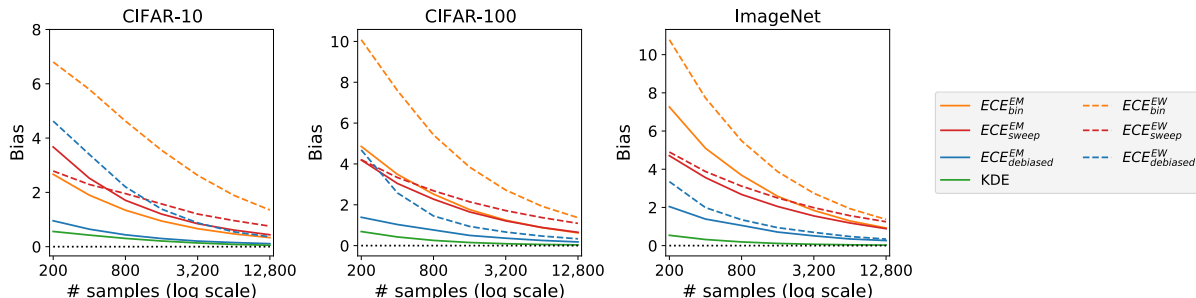
Figure 6: Perfectly calibrated models. Using BBC we set the calibration curve to have 0% calibration error but use realistic model confidence score distributions. We find that the KDE estimator has the least amount of bias for perfectly calibrated models, followed by ECE_{DEBIAS}^{EM}.

and if one has under 500 samples, the miscalibration must be greater than 10% to be detected reliably.

7.3 Perfect calibration

In Section 7.1, we studied realistic scenarios of models whose outputs have the same statistics as common neural architectures on popular datasets. The BBC framework also allows us to simulate a continuum of models that differ systematically in TCE. For all metrics, bias increases as TCE decreases (details in Appendix C). This finding is not surprising because binned metrics always produce a nonnegative ECE estimate, and in the limit of a perfectly calibrated model, any deviation of the binning histogram from the diagonal will result in positive bias.

In this section, we compare the bias of estimators for the case of a perfectly calibrated model—the ultimate aim of designing methods that minimize miscalibration. To simulate perfect calibration, the calibration curve of the model is set to $\mathbb{E}_Y[Y \mid f(X) = c] = c$, but we use the realistic confidence score distributions from the previous section.

Figure 6 illustrates the effect of sample size on bias for the seven different estimators under perfect calibration. Although the KDE estimator outperforms all others, it is not a viable candidate because it has a very high bias for realistic scenarios (Figure 4). Excluding KDE, ECE_{DEBIAS}^{EM} is the least biased metric, obtaining significantly lower bias than ECE_{SWEEP}^{EM}.

How do we reconcile these results with our previous finding (Figure 4) that ECE_{SWEEP}^{EM} is preferred over ECE_{DEBIAS}^{EM}? The present results assume a well calibrated model; the previous results are based on realistic scenarios. Whether one prefers ECE_{SWEEP}^{EM} or ECE_{DEBIAS}^{EM} ultimately depends on a practitioner's prior beliefs about a model's degree of miscalibration. But to some degree we are splitting hairs: both ECE_{SWEEP}^{EM} and ECE_{DEBIAS}^{EM} are consistently superior to common practice (ECE_{BIN}^{EW}) and proposed improvements (e.g.,

ECE_{DEBIAS}^{EW}, as recommended by Kumar et al., 2019).

8 DISCUSSION AND CONCLUSION

Calibration research typically focuses on recalibrating models, i.e., transforming $f(x)$ to $f'(x)$ (Platt et al., 1999; Zadrozny and Elkan, 2001, 2002). We focus on estimating true calibration error, because without a good estimate, how is one to select and evaluate recalibration methods? The preferred recalibration method for a given model and data set is affected by bias: Table 1 shows that using ECE_{SWEEP}^{EM} to select a recalibration method instead of ECE_{BIN}^{EW} leads to better choices and subsequently, better calibration on the test set. Indeed, bias may have impacted the conclusions of previous studies of calibration error, such as the well cited work of Guo et al. (2017). The choice of calibration error estimator can also impact the detection of miscalibration: Figure 5 indicates that ECE_{SWEEP}^{EM} is a more sensitive metric than ECE_{BIN}^{EW} for detecting if a model is miscalibrated.

Several authors attempt a different approach to recalibration: improving model calibration during training. For instance, Mukhoti et al. (2020) train a model with a batch size of 128 across multiple types of losses including maximum mean calibration error (Kumar et al., 2018) and Brier loss (Brier, 1950) which explicitly minimizes calibration loss using 128 examples at a time. However, our results suggest that training a model with naive estimates of calibration error using a batch size $< O(1000)$ is a potentially flawed endeavor, particularly because the distribution of scores from the model changes throughout training, and any potential calibration measure may be more affected by the distribution of scores than the true calibration curve.

Our work can be extended in many directions which we did not have space here to consider, including: examining violations of our distributions assumptions and the setting where the confidence-score distributions are less skewed; studying the interplay between bias and vari-

ance; exploring alternative task types, such as binary classification; and evaluating alternative calibration measures such as ℓ_1 TCE and KCE, KS, and MCE.

Relying on the predictions from machine learning models in high stakes situations like autonomous vehicles, content moderation, and medicine, requires the ability to detect predictions that are likely to be incorrect. Given that the default confidence scores produced by machine learning models do not necessarily correspond to the model's empirical accuracy, recalibration is necessary in order to produce reliable and consistent output. However, it is impossible to perfectly calibrate a model if calibration cannot be measured accurately. Our results show that the statistical bias in current calibration error estimators grows as we approach perfect calibration, but this bias can be mitigated by using equal-mass binning and methods such as the debiased estimator (Brocker, 2012; Ferro and Fricker, 2012; Kumar et al., 2019), $\text{ECE}^{\text{EM}}_{\text{DEBIAS}}$, or our own monotonic estimation technique, $\text{ECE}^{\text{EM}}_{\text{SWEEP}}$.

Acknowledgements

References

Azulay, A. and Weiss, Y. (2018). Why do deep convolutional networks generalize so poorly to small image transformations? *arXiv preprint arXiv:1805.12177*.

Biggio, B. and Roli, F. (2018). Wild patterns: Ten years after the rise of adversarial machine learning. *Pattern Recognition*. https://arxiv.org/abs/1712.03141.

Brier, G. W. (1950). Verification of forecasts expressed in terms of probability. *Monthly weather review*, 78(1):1–3.

Brocker, J. (2012). Estimating reliability and resolution of probability forecasts through decomposition of the empirical score. *Climate Dynamics*, 39:655–667.

Caesar, H., Bankiti, V., Lang, A. H., Vora, S., Liong, V. E., Xu, Q., Krishnan, A., Pan, Y., Baldan, G., and Beijbom, O. (2020). nuscenes: A multimodal dataset for autonomous driving. In *Proceedings of the IEEE/CVF Conference on Computer Vision and Pattern Recognition*, pages 11621–11631.

Chen, W., Sahiner, B., Samuelson, F., Pezeshk, A., and Petrick, N. (2018). Calibration of medical diagnostic classifier scores to the probability of disease. *Statistical methods in medical research*, 27(5):1394–1409.

Deng, J., Dong, W., Socher, R., Li, L.-J., Li, K., and Fei-Fei, L. (2009). ImageNet: A Large-Scale Hierarchical Image Database. In *CVPR09*.

Esteva, A., Kuprel, B., Novoa, R. A., Ko, J., Swetter, S. M., Blau, H. M., and Thrun, S. (2017). Dermatologist-level classification of skin cancer with deep neural networks. *nature*, 542(7639):115–118.

Esteva, A., Robicquet, A., Ramsundar, B., Kuleshov, V., DePristo, M., Chou, K., Cui, C., Corrado, G., Thrun, S., and Dean, J. (2019). A guide to deep learning in healthcare. *Nature medicine*, 25(1):24–29.

Ferro, C. A. T. and Fricker, T. E. (2012). A bias-corrected decomposition of the brier score. *Quarterly Journal of the Royal Meteorological Society*, 138:1954–1960.

Geiger, A., Lenz, P., Stiller, C., and Urtasun, R. (2013). Vision meets robotics: The kitti dataset. *The International Journal of Robotics Research*, 32(11):1231–1237.

Gelman, A., Carlin, J. B., Stern, H. S., and Rubin, D. B. (2004). *Bayesian Data Analysis*. Chapman and Hall/CRC, 2nd ed. edition.

Gneiting, T. and Vogel, P. (2018). Receiver operating characteristic (roc) curves. *arXiv preprint arXiv:1809.04808*.

Green, D. M., Swets, J. A., et al. (1966). *Signal detection theory and psychophysics*, volume 1. Wiley New York.

Gulshan, V., Peng, L., Coram, M., Stumpe, M. C., Wu, D., Narayanaswamy, A., Venugopalan, S., Widner, K., Madams, T., Cuadros, J., et al. (2016). Development and validation of a deep learning algorithm for detection of diabetic retinopathy in retinal fundus photographs. *Jama*, 316(22):2402–2410.

Guo, C., Pleiss, G., Sun, Y., and Weinberger, K. Q. (2017). On calibration of modern neural networks. *International Conference on Machine Learning (ICML)*.

Gupta, K., Rahimi, A., Ajanthan, T., Mensink, T., Sminchisescu, C., and Hartley, R. (2020). Calibration of neural networks using splines. *arXiv preprint arXiv:2006.12800*.

He, K., Zhang, X., Ren, S., and Sun, J. (2016). Deep residual learning for image recognition. In *Computer Vision and Pattern Recognition (CVPR)*.

Hendrycks, D. and Dietterich, T. (2019). Benchmarking neural network robustness to common corruptions and perturbations. In *International Conference on Learning Representations (ICLR)*. https://arxiv.org/abs/1807.01697.

Huang, G., Liu, Z., Van Der Maaten, L., and Weinberger, K. Q. (2017). Densely connected convolu-

tional networks. In *Proceedings of the IEEE conference on computer vision and pattern recognition*, pages 4700–4708.

Huang, G., Sun, Y., Liu, Z., Sedra, D., and Weinberger, K. Q. (2016). Deep networks with stochastic depth. In *European conference on computer vision*, pages 646–661. Springer.

Karandikar, A., Cain, N., Tran, D., Lakshminarayanan, B., Shlens, J., Mozer, M. C., and Roelofs, B. (2021). Soft calibration objectives for neural networks. In *Advances in Neural Information Processing Systems*.

Krishnan, R. and Tickoo, O. (2020). Improving model calibration with accuracy versus uncertainty optimization. *ArXiv*, abs/2012.07923.

Krizhevsky, A. and Hinton, G. (2009). Learning multiple layers of features from tiny images. Technical report, University of Toronto, Department of Computer Science.

Kumar, A., Liang, P. S., and Ma, T. (2019). Verified uncertainty calibration. In *Neural Information Processing Systems (NeurIPS)*.

Kumar, A., Sarawagi, S., and Jain, U. (2018). Trainable calibration measures for neural networks from kernel mean embeddings. In *International Conference on Machine Learning (ICML)*, pages 2805–2814.

Kängsepp, M. (2019). Nn_calibration. https://github.com/markus93/NN_calibration.

LeCun, Y., Bottou, L., Bengio, Y., and Haffner, P. (1998). Gradient-based learning applied to document recognition. *Proceedings of the IEEE*, 86(11):2278–2324.

Lin, T.-Y., Goyal, P., Girshick, R., He, K., and Dollár, P. (2018). Focal loss for dense object detection.

Mukhoti, J., Kulharia, V., Sanyal, A., Golodetz, S., Torr, P. H., and Dokania, P. K. (2020). Calibrating deep neural networks using focal loss. *arXiv preprint arXiv:2002.09437*.

Naeini, M. P., Cooper, G. F., and Hauskrecht, M. (2015). Obtaining well calibrated probabilities using bayesian binning. In *AAAI Conference on Artificial Intelligence*. NIH Public Access.

Nixon, J., Dusenberry, M. W., Zhang, L., Jerfel, G., and Tran, D. (2019). Measuring calibration in deep learning. In *CVPR Workshops*, pages 38–41.

Pesce, L. L., Metz, C. E., and Berbaum, K. S. (2010). On the convexity of roc curves estimated from radiological test results. *Academic radiology*, 17(8):960–968.

Platt, J. et al. (1999). Probabilistic outputs for support vector machines and comparisons to regularized likelihood methods. *Advances in large margin classifiers*, 10(3):61–74.

Recht, B., Roelofs, R., Schmidt, L., and Shankar, V. (2019). Do imagenet classifiers generalize to imagenet? In *International Conference on Machine Learning*, pages 5389–5400.

Sun, P., Kretzschmar, H., Dotiwalla, X., Chouard, A., Patnaik, V., Tsui, P., Guo, J., Zhou, Y., Chai, Y., Caine, B., et al. (2020). Scalability in perception for autonomous driving: Waymo open dataset. In *Proceedings of the IEEE/CVF Conference on Computer Vision and Pattern Recognition*, pages 2446–2454.

Szegedy, C., Zaremba, W., Sutskever, I., Bruna, J., Erhan, D., Goodfellow, I. J., and Fergus, R. (2013). Intriguing properties of neural networks. In *International Conference on Learning Representations (ICLR)*. http://arxiv.org/abs/1312.6199.

Widmann, D., Lindsten, F., and Zachariah, D. (2019). Calibration tests in multi-class classification: A unifying framework. *NeurIPS*.

Wu, Y., Jiang, X., Kim, J., and Ohno-Machado, L. (2012). I-spline smoothing for calibrating predictive models. *AMIA Summits on Translational Science Proceedings*, 2012:39.

Zadrozny, B. and Elkan, C. (2001). Obtaining calibrated probability estimates from decision trees and naive bayesian classifiers. In *Icml*, volume 1, pages 609–616. Citeseer.

Zadrozny, B. and Elkan, C. (2002). Transforming classifier scores into accurate multiclass probability estimates. In *ACM SIGKDD International Conference on Knowledge Discovery and Data Mining*.

Zagoruyko, S. and Komodakis, N. (2016). Wide residual networks. *arXiv preprint arXiv:1605.07146*.

Zhang, J., Kailkhura, B., and Han, T. (2020). Mix-n-match: Ensemble and compositional methods for uncertainty calibration in deep learning. *arXiv preprint arXiv:2003.07329*.

A Maximum-likelihood fits

A.1 Confidence score distribution fits

Table 2 provides parameters of best fit for the Beta distribution for each of 10 empirical datasets, obtained by fitting the top-label confidence score via maximum likelihood estimation.

Table 2: Parameters of best fit for Beta distribution investigated in Section 6.

	$\hat{\alpha}$	$\hat{\beta}$
resnet110_c10	2.7752	0.0478
resnet110_SD_c10	2.1714	0.0394
resnet_wide32_c10	2.3806	0.0379
densenet40_c10	1.9824	0.0397
resnet110_c100	1.1823	0.1081
resnet110_SD_c100	1.1233	0.1147
resnet_wide32_c100	1.0611	0.0650
densenet40_c100	1.0805	0.0808
resnet152_imgnet	1.1359	0.2069
densenet161_imgnet	1.1928	0.2206

Global optimia $\hat{\alpha} \in [0, 200]$, $\hat{\beta} \in [0, 50]$ are approximately computed using a recursively-refining brute-force search until both parameters are established to within an absolute tolerance of 1e−5. Each step in the recursion contracts a linear sampling grid ($N = 11$) by a factor of $\gamma = .5$ centered on the previously established optimal parameter, subject to the constraints $\alpha, \beta > 0$. Experiments confirmed that the computed optima were robust to the hyperparameters N, γ.

$$\arg\min_{\alpha,\beta} \sum_i - \ln \frac{x_i^{\alpha-1}(1 - x_i)^{\beta-1}}{\frac{\Gamma(\alpha)\Gamma(\beta)}{\Gamma(\alpha+\beta)}} \qquad (9)$$

A.2 Calibration curve fits

Table 3 provides parameters fit to calibration functions. For each sample image x_i in the image dataset, define $s_i = f(x_i)$ to be the score (the output of the top-scoring logit after softmax) and $y_i \in \{0, 1\}$ to be the classification ($y_i = 1$ when the top-scoring logit correctly classified image x_i) for the sample image. The loss for the binary generalized linear model (GLM) across different combinations of link functions $g(y)$ and transform functions $t(s)$ was optimized via the standard loss (Gelman et al., 2004):

$$\arg\min_{b_0,b_1} \sum_i - \ln p_i^{y_i}(1-p_i)^{1-y_i}, \quad p_i = g^{-1}(b_0+b_1 t(s_i)) \qquad (10)$$

For each dataset, the GLM of best fit was selected via the Akaike Information Criteria using the likelihood at the optimized parameter values.

A.3 Comparing ECE$_{\text{BIN}}$ computed on simulated data versus real data

In Figure 3c, we compare the ECE$_{\text{BIN}}$ computed on the original logit output of each model to the average ECE$_{\text{BIN}}$ we obtain after sampling 1,000 simulated datasets from our parametric fits. Table 4 reports the ECE$_{\text{BIN}}$ measurements that we plot in Figure 3. We observe that the two measurements of ECE$_{\text{BIN}}$ are relatively close, indicating that our parametric models are well-fit to the original data.

Table 3: Parameters of best fit for calibrations functions investigated in Section 6 (table continues on next page).

dataset_name	glm_name	AIC	b_0	b_1
resnet110_c10	logflip_logflip_b0_b1	**2779.22**	-0.24	0.30
	logit_logflip_b0_b1	2790.40	-0.55	-0.38
	logit_logflip_b1	2827.51		-0.31
	logit_logit_b0_b1	2840.70	-0.38	0.36
	logit_logit_b1	2900.02		0.30
	logflip_logflip_b1	2932.09		0.34
	log_log_b0_b1	3221.72	-0.06	2.53
	logit_logit_b0	3799.63	1.99	
	logflip_logflip_b0	3811.98	-2.13	
	log_log_b0	3829.05	-0.13	
	logit_logflip_b0	3868.40	1.95	
	log_log_b1	4281.78		4.75
resnet110_SD_c10	logit_logflip_b0_b1	**2498.98**	-0.27	-0.35
	logit_logit_b1	2502.52		0.30
	logit_logflip_b1	2508.70		-0.30
	logit_logit_b0_b1	2538.41	-0.26	0.33
	logflip_logflip_b0_b1	2550.29	-0.36	0.27
	logflip_logflip_b1	2572.85		0.35
	log_log_b0_b1	2594.91	-0.08	1.98
	log_log_b0	3137.19	-0.19	
	logflip_logflip_b0	3150.42	-1.80	
	logit_logit_b0	3175.58	1.58	
	logit_logflip_b0	3179.67	1.56	
	log_log_b1	3697.37		3.77
resnet_wide32_c10	logit_logit_b1	**2483.34**		0.26
	logflip_logflip_b0_b1	2487.69	-0.47	0.22
	logit_logit_b0_b1	2511.39	-0.13	0.28
	logit_logflip_b0_b1	2558.45	-0.26	-0.28
	logit_logflip_b1	2586.47		-0.25
	log_log_b0_b1	2647.03	-0.12	1.87
	logflip_logflip_b1	2713.17		0.30
	log_log_b0	2981.24	-0.21	
	logflip_logflip_b0	2983.05	-1.70	
	logit_logit_b0	2989.90	1.49	
	logit_logflip_b0	3055.55	1.45	
	log_log_b1	4582.09		4.61
densenet40_c10	logit_logflip_b1	**2910.62**		-0.26
	logit_logit_b0_b1	2961.31	-0.40	0.31
	logit_logflip_b0_b1	3000.23	-0.38	-0.31
	logflip_logflip_b0_b1	3001.78	-0.31	0.24
	logit_logit_b1	3021.54		0.25
	logflip_logflip_b1	3027.78		0.31
	log_log_b0_b1	3153.38	-0.12	2.04
	log_log_b0	3531.22	-0.22	
	logflip_logflip_b0	3589.11	-1.60	
	logit_logit_b0	3601.85	1.37	
	logit_logflip_b0	3679.95	1.30	
	log_log_b1	4735.18		4.27
resnet110_c100	logflip_logflip_b0_b1	**8181.97**	-0.11	0.28
	logit_logit_b0_b1	8206.19	-0.88	0.39
	logflip_logflip_b1	8301.28		0.31
	logit_logflip_b0_b1	8371.53	-1.01	-0.40
	logit_logit_b1	8732.11		0.25
	log_log_b0_b1	8918.21	-0.16	2.35
	logit_logflip_b1	8926.99		-0.23
	logit_logflip_b0	10903.83	0.74	
	logit_logit_b0	10943.95	0.72	
	logflip_logflip_b0	10964.91	-1.12	
	log_log_b0	11002.20	-0.40	
	log_log_b1	11850.89		4.26

dataset_name	glm_name	AIC	b_0	b_1
resnet110_SD_c100	logit_logit_b0_b1	**7873.61**	-0.88	0.49
	logflip_logflip_b0_b1	7878.19	-0.09	0.35
	logflip_logflip_b1	7932.28		0.38
	logit_logflip_b0_b1	7944.61	-1.04	-0.52
	logit_logit_b1	8315.51		0.32
	log_log_b0_b1	8437.82	-0.11	2.18
	logit_logflip_b1	8510.36		-0.30
	log_log_b1	9988.07		3.30
	logit_logit_b0	10803.27	0.80	
	log_log_b0	10810.90	-0.37	
	logflip_logflip_b0	10823.15	-1.16	
	logit_logflip_b0	10834.48	0.78	
resnet_wide32_c100	logflip_logflip_b0_b1	**7183.93**	-0.13	0.21
	logit_logit_b0_b1	7219.14	-0.98	0.33
	logflip_logflip_b1	7233.51		0.25
	logit_logflip_b0_b1	7297.00	-1.06	-0.34
	logit_logit_b1	7626.21		0.19
	log_log_b0_b1	7650.97	-0.24	2.51
	logit_logflip_b1	7795.28		-0.17
	logflip_logflip_b0	8977.39	-0.98	
	logit_logflip_b0	8987.38	0.49	
	log_log_b0	9000.24	-0.49	
	logit_logit_b0	9009.51	0.49	
	log_log_b1	11911.51		5.48
densenet40_c100	logit_logit_b0_b1	**8158.28**	-0.97	0.34
	logflip_logflip_b0_b1	8229.43	-0.12	0.22
	logit_logflip_b0_b1	8267.77	-1.08	-0.35
	logflip_logflip_b1	8368.86		0.25
	logit_logit_b1	8783.50		0.19
	log_log_b0_b1	8832.20	-0.25	2.26
	logit_logflip_b1	8918.57		-0.18
	logit_logit_b0	10138.24	0.47	
	logit_logflip_b0	10182.61	0.45	
	logflip_logflip_b0	10242.15	-0.94	
	log_log_b0	10261.01	-0.50	
	log_log_b1	13322.10		5.25
resnet152_imgnet	logflip_logflip_b0_b1	**18729.85**	-0.12	0.58
	logit_logit_b0_b1	18783.22	-0.29	0.65
	log_log_b0_b1	18785.44	-0.03	1.32
	logflip_logflip_b1	18872.14		0.65
	logit_logit_b1	19074.37		0.57
	logit_logflip_b0_b1	19095.40	-0.82	-0.79
	log_log_b1	19840.25		1.53
	logit_logflip_b1	20062.10		-0.50
	logflip_logflip_b0	26935.09	-1.41	
	log_log_b0	26968.50	-0.28	
	logit_logflip_b0	27012.77	1.12	
	logit_logit_b0	27084.11	1.11	
densenet161_imgnet	log_log_b0_b1	**18202.41**	-0.03	1.27
	logit_logit_b0_b1	18460.70	-0.25	0.68
	logflip_logflip_b1	18521.48		0.67
	logflip_logflip_b0_b1	18534.07	-0.10	0.61
	logit_logit_b1	18822.25		0.60
	logit_logflip_b0_b1	18913.25	-0.77	-0.80
	log_log_b1	19493.85		1.44
	logit_logflip_b1	19562.58		-0.54
	logit_logflip_b0	26426.38	1.19	
	logflip_logflip_b0	26445.91	-1.46	
	logit_logit_b0	26519.76	1.18	
	log_log_b0	26662.65	-0.27	

Table 4: $\mathrm{ECE_{BIN}}$ reported in Figure 3c.

	$\mathrm{ECE_{BIN}}$ (%)	$<\mathrm{ECE_{BIN}}>$ (%, simulated)
resnet110_c10	6.67	8.42
resnet110_SD_c10	6.54	8.79
resnet_wide32_c10	6.09	8.44
densenet40_c10	6.70	8.09
resnet110_c100	20.26	18.87
resnet110_SD_c100	17.44	15.78
resnet_wide32_c100	20.40	17.53
densenet40_c100	23.12	19.69
resnet152_imgnet	6.85	9.26
densenet161_imgnet	6.15	6.87

B Bias and variance in calibration metrics

B.1 Bias

We evaluate bias for various calibration metrics using both equal-width and equal-mass binning as we vary both the sample size n and the number of bins b. These plots should be seen as an alternative visualization to 4 where we additionally compare to different choices for the fixed number of bins b. Since the $\text{ECE}_{\text{SWEEP}}$ metrics adaptively choose a different number of bins for each sample size, we display the bin number for this metric as -1.

We find that ECE_{BIN} can overestimate the true calibration error and there exists an optimal number of bins that produces the least biased estimator that changes with the number of samples n. Additionally, equal mass binning generally results in a less biased metric than equal width binning.

CIFAR-10 ResNet-110. Figure 7 assume parametric curves for $p(f(x))$ and $\mathbb{E}_Y[Y \mid f(X) = c]$ that we obtain from maximum-likelihood fits to CIFAR-10 ResNet-110 model output.

CIFAR-100 Wide ResNet-32. Figure 8 assume parametric curves for $p(f(x))$ and $\mathbb{E}_Y[Y \mid f(X) = c]$ that we obtain from maximum-likelihood fits to CIFAR-100 Wide ResNet-32 model output.

ImageNet ResNet-152. Figure 9 assume parametric curves for $p(f(x))$ and $\mathbb{E}_Y[Y \mid f(X) = c]$ that we obtain from maximum-likelihood fits to ImageNet ResNet-152 model output.
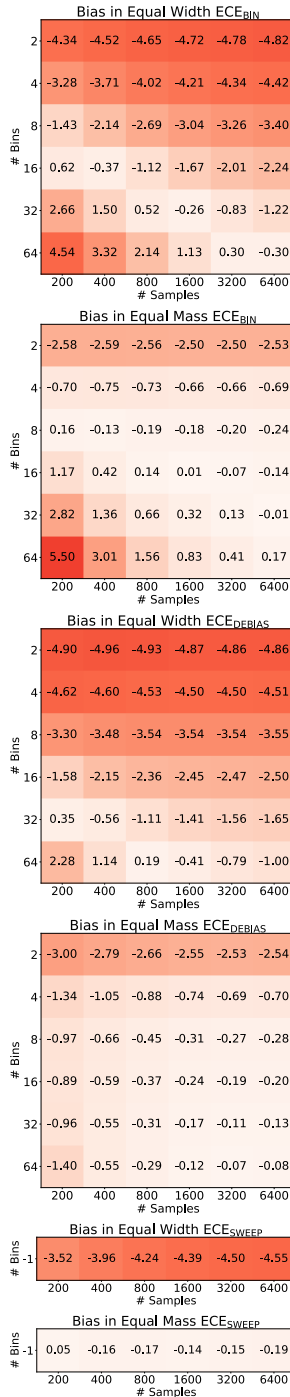
Figure 7: **Bias for various calibration metrics assuming curves fit to CIFAR-10 ResNet-110 output.** We plot bias for various calibration metrics using both equal-width binning (left column) and equal-mass binning (right column) as we vary both the sample size n and the number of bins b.
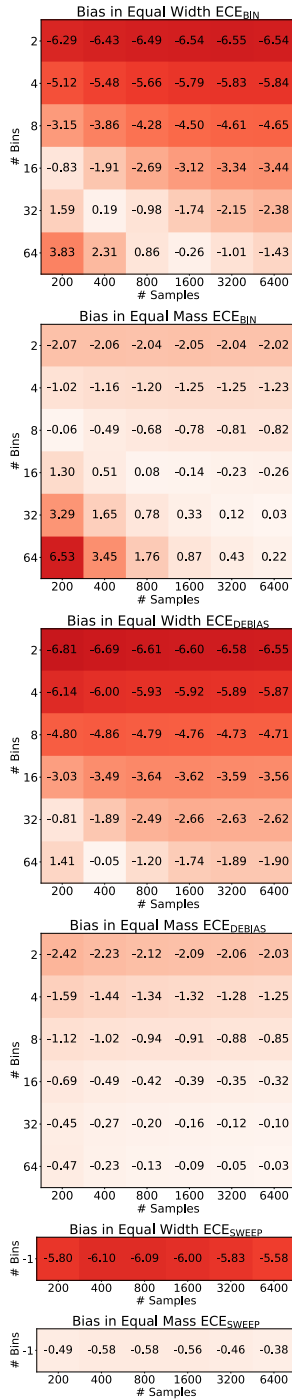
Figure 8: **Bias for various calibration metrics assuming curves fit to CIFAR-100 Wide ResNet-32 output.** We plot bias for various calibration metrics using both equal-width binning (left column) and equal-mass binning (right column) as we vary both the sample size n and the number of bins b.
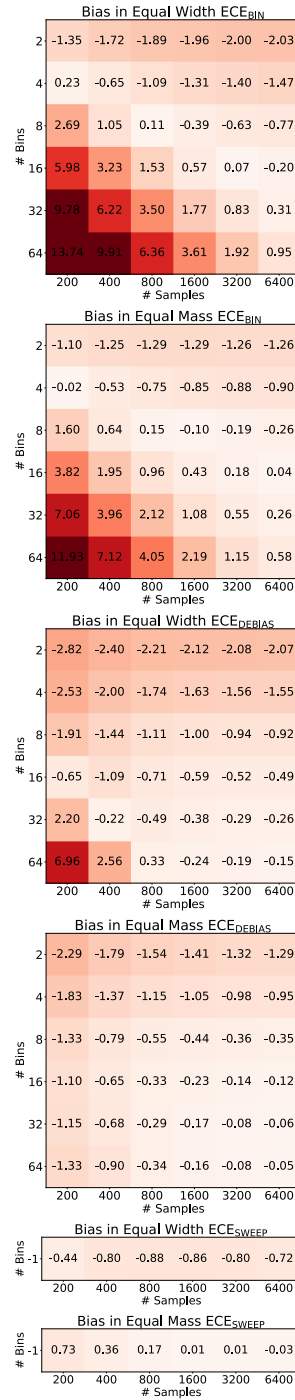
Figure 9: **Bias for various calibration metrics assuming curves fit to ImageNet ResNet-152 output.** We plot bias for various calibration metrics using both equal-width binning (left column) and equal-mass binning (right column) as we vary both the sample size n and the number of bins b.
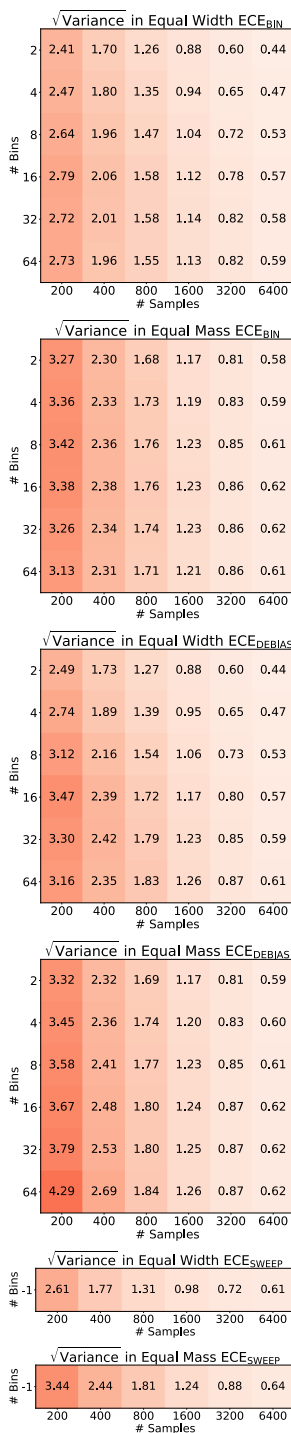
B.2 Variance

We also compute the *variance* for various calibration metrics using both equal-width and equal-mass binning as we vary both the sample size n and the number of bins b. As expected, the variance decreases with number of samples, but, unlike the bias, there is no clear dependence on the number of bins.

CIFAR-10 ResNet-110. Figure 10 assume parametric curves for $p(f(x))$ and $\mathbb{E}_Y[Y \mid f(X) = c]$ that we obtain from maximum-likelihood fits to CIFAR-10 ResNet-110 model output.

CIFAR-100 Wide ResNet-32. Figure 11 assume parametric curves for $p(f(x))$ and $\mathbb{E}_Y[Y \mid f(X) = c]$ that we obtain from maximum-likelihood fits to CIFAR-100 Wide ResNet-32 model output.

ImageNet ResNet-152. Figure 12 assume parametric curves for $p(f(x))$ and $\mathbb{E}_Y[Y \mid f(X) = c]$ that we obtain from maximum-likelihood fits to ImageNet ResNet-152 model output.
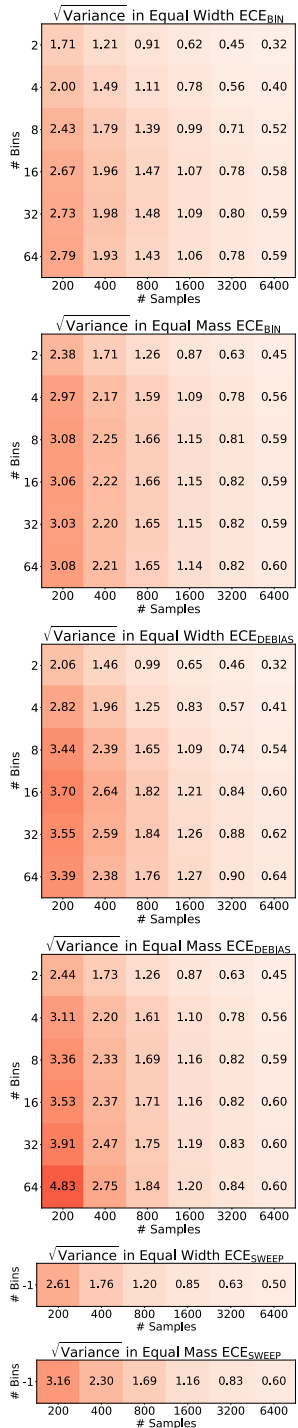
Figure 10: $\sqrt{\textbf{Variance}}$ **for various calibration metrics assuming curves fit to CIFAR-10 ResNet-110 output.** We plot $\sqrt{\text{Variance}}$ for various calibration metrics using both equal-width binning (left column) and equal-mass binning (right column) as we vary both the sample size n and the number of bins b.
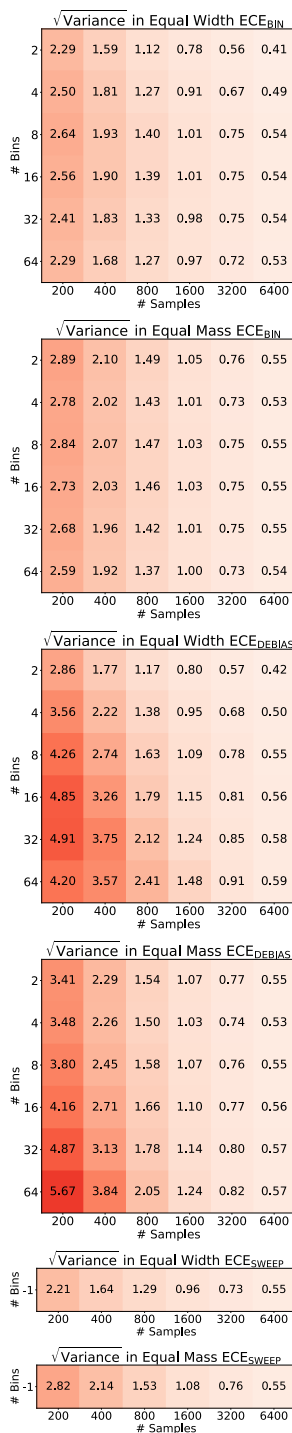
Figure 11: √**Variance for various calibration metrics assuming curves fit to CIFAR-100 Wide ResNet-32 output.** We plot √Variance for various calibration metrics using both equal-width binning (left column) and equal-mass binning (right column) as we vary both the sample size n and the number of bins b.

Figure 12: √**Variance for various calibration metrics assuming curves fit to ImageNet ResNet-152 output.** We plot √Variance for various calibration metrics using both equal-width binning (left column) and equal-mass binning (right column) as we vary both the sample size n and the number of bins b.

C Controlling true calibration error using BBC

We evaluate the estimation bias of calibration estimators as we systematically vary the TCE. Figure 13 shows the average estimated calibration error for $\text{ECE}_{\text{BIN}}^{\text{EW}}$ and $\text{ECE}_{\text{SWEEP}}^{\text{EM}}$ versus the TCE. The average calibration error is computed across $m = 1,000$ simulated datasets, and we include results for two sample sizes, $n = 200$ and $n = 5,000$, and two score distributions, $f(x) \sim \text{Uniform}(0,1)$ and $f(x) \sim \text{Beta}(1.1, 0.1)$, the beta distribution fit to the CIFAR-100 Wide ResNet_32. To control the TCE, we assume $\mathbb{E}_Y[Y \mid f(X) = c] = c^d$ and vary $d \in [1, 10]$. When $d = 1$ the true calibration curve is $\mathbb{E}_Y[Y \mid f(X) = c] = c$, which means the model's predicted confidence score is exactly equal to its empirical accuracy and thus the TCE is 0%. As we increase d, we move the true calibration curve farther away from the perfect calibration curve, which increases the TCE of the model.

The estimation bias can be seen visually as the difference between the ECE and the $y = x$ line. Perfect estimation (0 bias) corresponds to the $y = x$ line. Bias is highest when the model is perfectly calibrated (TCE is 0%) and generally decreases as TCE increases. A larger sample size of $n = 5,000$ reduces the bias, but with perfectly calibration ECE_{BIN} can still be off by 2%. The $\text{ECE}_{\text{SWEEP}}^{\text{EM}}$ metric significantly reduces this bias.

D What number of bins does $\text{ECE}_{\text{SWEEP}}^{\text{EM}}$ choose?

For Figure 14, the uncalibrated plot assumes $\mathbb{E}_Y[Y \mid f(X) = c] = \text{logistic}(10 * c - 5)$ while the calibrated
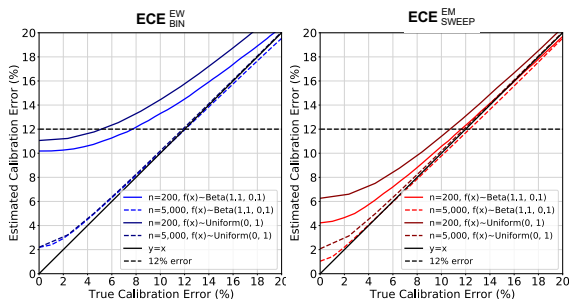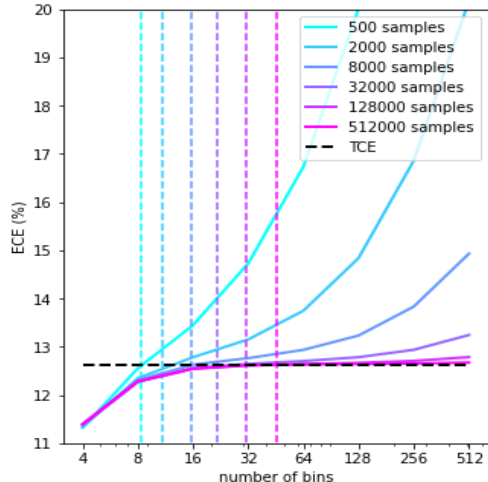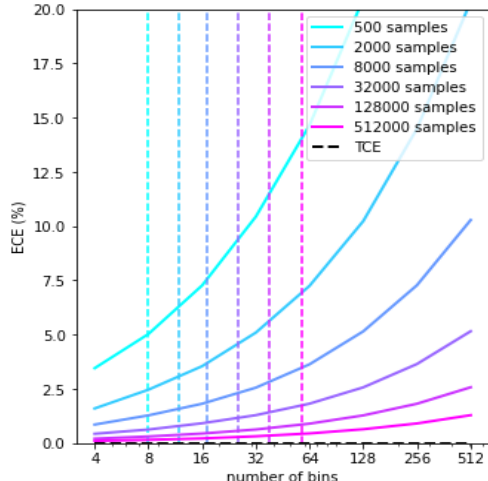

(a) Uncalibrated model.

(b) Perfectly calibrated model.

Figure 14: **Bins chosen by equal mass $\text{ECE}_{\text{SWEEP}}$ method**. We plot equal mass ECE_{BIN} % versus number of bins for various sample sizes n. We highlight the TCE with a horizontal dashed line and show the average number of bins chosen by the $\text{ECE}_{\text{SWEEP}}$ method for different sample sizes with vertical dashed lines. When the model is uncalibrated (left) $\text{ECE}_{\text{SWEEP}}$ chooses a bin number that is close to optimal. However, for perfectly calibrated models (right), the optimal number of bins is small ($<=4$), and $\text{ECE}_{\text{SWEEP}}$ does not do a good job of selecting a good bin number. The incorrect bin selection may partially explain why $\text{ECE}_{\text{SWEEP}}$ still has some bias for perfectly calibrated models. However, we note that any binning-based technique that always outputs a positive number will never be completely unbiased for perfectly calibrated models.

Figure 13: Bias in calibration estimation increases as TCE decreases. Average ECE (%) for $\text{ECE}_{\text{BIN}}^{\text{EW}}$ (left) and $\text{ECE}_{\text{SWEEP}}^{\text{EM}}$ (right) versus the TCE (%), with varying sample size and score distributions. The estimator bias is systematically worse for better calibrated models, and the effect is more egregious with fewer samples. At $n = 200$ samples, depending on the score distribution, an $\text{ECE}_{\text{BIN}}^{\text{EW}}$ estimate of 12% could either correspond to 5% or 8% TCE. $\text{ECE}_{\text{SWEEP}}^{\text{EM}}$ somewhat mitigates the bias and ambiguity in calibration error estimation.

plot assumes $\mathbb{E}_Y[Y \mid f(X) = c] = c$. Both experiments assume $f(x) \sim \text{Uniform}(0,1)$.